A Robotic Endoscopic Injection Needle with Integrated Tactile Sensor for Intraoperative Autonomous Tumor Localization

Yan Hong[1], Yingxuan Zhang[1], Chengjun Zhu[2], and Feng Ju[1(✉)]

[1] College of Mechanical and Electrical Engineering, Nanjing University of Aeronautics and Astronautics, Nanjing 210016, China
juf@nuaa.edu.cn

[2] Department of Oncology, Jiangsu Province Hospital, Nanjing 210029, China

Abstract. En bloc resection of tumor is a minimally invasive surgical method for removing tumors precisely and completely at one time. It can decrease the risk of recurrence and tumor spread after surgery. However, it requires surgeons to accurately locate the tumor and its boundary. In minimally invasive surgery (MIS), surgeons cannot directly palpate cancerous areas to obtain tactile information. Therefore, a tactile sensor that can be integrated onto surgical instruments is highly demanded. This paper proposes a tactile sensor integrated onto an injection needle for robotic endoscopes. The tactile sensor is based on the principle of piezoelectric effect and can detect the hardness of tissues by changes of resonant frequency. In addition, an autonomous palpation algorithm is developed to accurately localize the tumor and identify its boundaries.

Keywords: Tactile sensor · Tumor palpation · Robotic endoscope · Autonomous tumor localization · Injection needle

1 Introduction

En bloc resection is a kind of minimally invasive surgical method to remove a tumor at one time. This method can effectively decrease the possibility of postoperative recurrence. It lifts the tumor by injecting sodium hyaluronate, and then completely separates it from healthy tissue by an electrosurgical knife [1]. It requires surgeons to accurately locate the tumor and its boundary. If the location of the tumor cannot be accurately detected, surgeons may possibly remove healthy tissues as tumors. It maybe causes massive bleeding and endangers the lives of patients. However, the surgeon cannot directly palpate the cancerous area with hands. Therefore, it is necessary to design a tactile sensor to assist surgeons in acquiring the location of the tumor. Up to now, tactile sensors based on various principles have been developed.

X.-J. Liu et al. (Eds.): ICIRA 2021, LNAI 13015, pp. 165–176, 2021.
https://doi.org/10.1007/978-3-030-89134-3_16

Zareinia et al. [2] developed a force-sensing bipolar forceps based on piezoresistive principle for quantifying the force between surgical instruments and tissues in microsurgery. In a recent study, Sharma et al. [3] developed a biopsy needle integrated with a piezoelectric sensor that can detect changes of tissue hardness. Kim et al. [4] proposed a novel perceptual surgical forceps consisting of two compact capacitive sensors located on two jaws of the forceps. It provides the surgeon with force and torque information. Tanaka et al. [5] proposed a tactile sensor based on acoustic reflection. By measuring the change of acoustic wave amplitude in the pipe, the sensor can obtain the deformation when contacting with the tissue. In recent years, fiber Bragg grating (FBG) has been widely used in tactile sensors. Li et al. [6] proposed a triaxial tactile sensor based on FBG for surface reactivity mapping, recognition and localization of tissue hard inclusion. However, all tactile sensors mentioned above require a force large enough to squeeze the tissue to generate a significant deformation for measurement, which may cause damage to living tissues. In [7, 8], a piezoelectric sensor was proposed to detect the hardness of tissue through the change of its resonant frequency when contacting with the tissue. In this way, the deformation of tissue can be reduced and tissue damage can be avoided. However, the integration of this sensor with existing surgical instruments remains a problem to solve.

The paper proposes a tactile sensor which can be easily integrated onto a robotic endoscopic injection needle. It can detect tissue hardness by the change of resonant frequency. A boundary recognition algorithm is proposed for accurately detecting the tumor location and its boundary, which is suitable for en bloc tumor resection. Section 2 introduces the structure and working principle of the sensor. Section 3 verifies the detection performance of the sensor through a series of simulation studies. Section 4 presents the principle of boundary recognition algorithm and its simulation results.

2 Design of the Tactile Sensor

2.1 Structure of the Tactile Sensor

The structure of the tactile sensor is shown in Fig. 1. It consists of a PZT (Pbbased Lanthanumdoped Zirconate Titanates) patch and a small stainless steel tip. One end of the PZT patch is fixed on the needle sheath. The tip is fixed on the other end of the PZT and contacts with the injection needle. This configuration adds the tactile sensing capability to the disposable injection needle without affecting its medical functions. In the tactile sensing mode, the tip of the injection needle is controlled by the robotic endoscope (e.g. a continuum robot) to contact with the tissue. Then the hardness of tissue is sensed by the PZT patch based on the following principle.

2.2 Hardness Sensing Principle

Due to the inverse piezoelectric effect, as shown in Fig. 2(a), when an AC voltage is applied to the electrode of a Y-axis polarized PZT patch, periodic expansion and contraction movements will occur in the X-axis. As a result, the tip of the injection

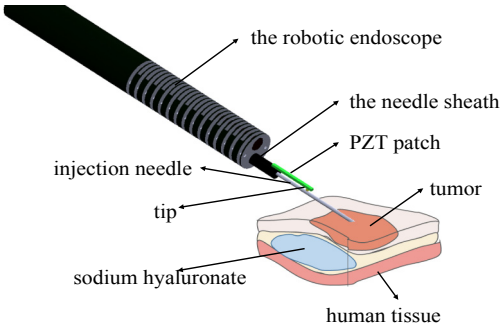

Fig. 1. Structure of the tactile sensor and the application in en bloc tumor resection.

needle will be excited to vibrate in the Y-axis. According to the equivalent circuit model in Fig. 2(b), the electrical impedance Z_e of the PZT patch can be expressed as:

$$Z_e = \frac{\left(L_1C_1\omega^2 - 1\right) - j(R_1C_1\omega)}{\left(R_1C_1C_0\omega^2\right) + \left[L_1C_0C_1\omega^3 - \omega(C_1{+}C_0)\right]} = |Ze(\omega)|\angle\theta(\omega) \tag{1}$$

where C_0 is the electrical capacitance, R_1 is the mechanical dissipation, L_1 is the mechanical mass, C_1 is the mechanical compliance, and ω is the frequency [9]. When the sensor is excited at its resonant frequency ω_R, the amplitude of its electrical impedance $|Ze(\omega)|$ reaches a local minimum which can be used to extract the ω_R (Fig. 2(c)). When the sensor is in contact with the tissue, its resonant frequency will change due to the change of the mechanical compliance C_1 (related to the hardness of the tissue). Therefore, tissue hardness can be measured from the resonant frequency of the sensor.

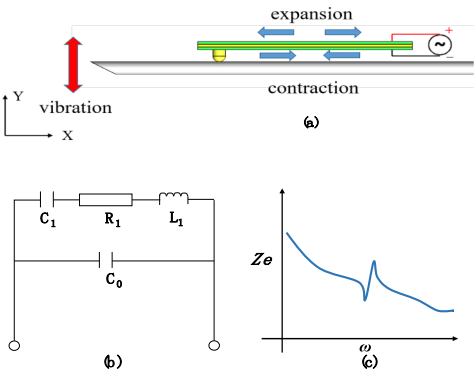

Fig. 2. (a) Principle of hardness sensing by simultaneous actuation and sensing capability of the sensor. (b) Equivalent circuit. (c) Electrical impedance - frequency curve.

3 Simulation Studies

3.1 Static Simulation for Verifying Whether the Sensor Damages Tissue

A finite element model of the sensor is built for simulation. The dimensions and materials are listed in Table 1.

Table 1. Dimensions and materials of the FE model

Component	Dimensions	Material
Piezo bimorph upper layer	10 × 0.7 × 0.15 mm	PZT-5A
Piezo bimorph substrate	10 × 0.7 × 0.15 mm	Brass
Piezo bimorph lower layer	10 × 0.7 × 0.15 mm	PZT-5A
Tip	Diameter 0.6 mm	Stainless steel
Injection needle	Diameter 0.75 mm	Stainless steel
Needle sheath	Diameter 2.4 mm	Stainless steel
Sample	10 × 10 × 3 mm	Silicone

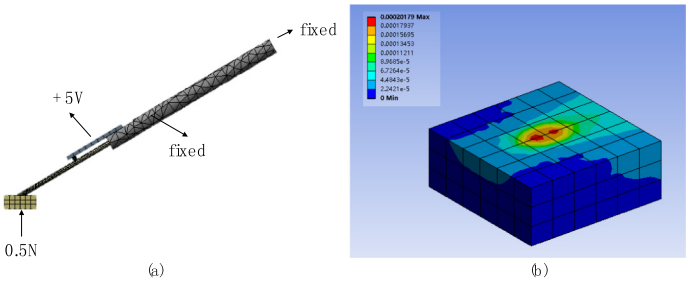

Fig. 3. (a) Boundary condition setting. (b) The deformation of the sample

For the boundary conditions, we fixed the upper end of the injection needle and the upper end of the needle sheath. At the same time, we applied a voltage of 5 V on the upper layer of the PZT patch for driving the PZT. Simultaneously, the contact between the tip and the injection needle is set to bonding, and the boundary condition between the injection needle and the sample is also set to bonding. In addition, in order to make the sensor better contact with the tissue model, a force of 0.5 N was applied to the sample (shown in Fig. 3(a)). The maximum deformation of the sensor is 0.2 mm, so it will not damage the tissue when detecting the hardness (shown in Fig. 3(b)).

3.2 Harmonic Response Simulation of Tissue Hardness Detection

Since the paper mainly studies the relationship between the sensor's resonant frequency and the hardness of the tissue, five tissue models with different elastic modulus are set for simulation, shown in Table 2.

For each tissue model, a 5 V swept sinusoidal voltage signal with a frequency range of 900–2300 Hz was applied to the two electrodes of the PZT patch in the sensor to drive the PZT patch to vibrate and its electrical impedance curve was recorded.

Table 2. Sample number and hardness

Sample number	Hardness (MPa)
1	0.157
2	0.228
3	0.414
4	0.6
5	0.883

The electrical impedance curves corresponding to different tissue models are shown in Fig. 4. The frequency corresponding to the lowest part of the curve is the resonant frequency of the sensor. It can be seen from the figure that the resonant frequency of the sensor changes when it is in contact with tissues with different elastic modulus. The bigger the elastic modulus, the higher the resonant frequency. It can be seen that the sensor has the function of identifying tissues with different hardness.

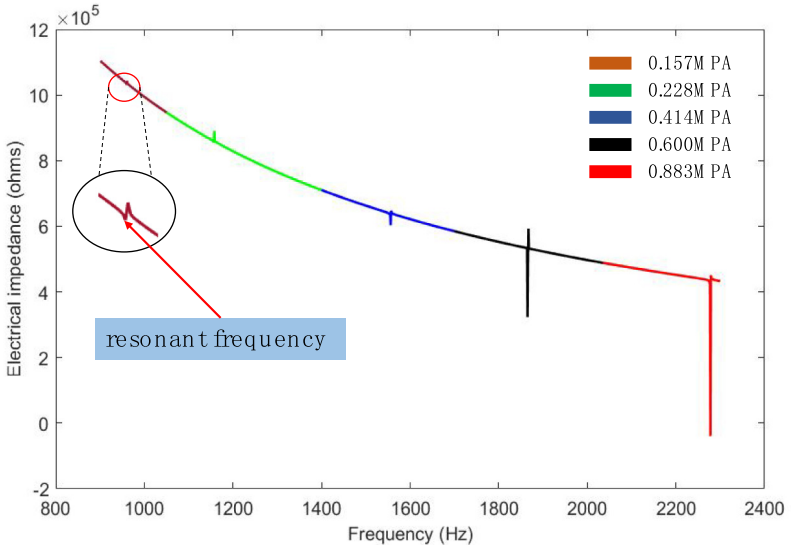

Fig. 4. The curve of electrical impedance-frequency shifts to the right under different hardness.

3.3 Sensor Performance Simulation Under Different Contact Angles

Disposable injection needles for endoscopes cannot ensure that the tip of the needle fits closely with the tissue due to the limited field of view during MIS. Therefore, we need to consider the impact of different contact angles on sensor performance.

We set up 5 tissue samples with different hardness, including one normal tissue and four high-hardness tissues as tumors. The hardness of the tissue samples is shown in Table 3 below. The elastic modulus of normal tissue refers to the hardness of muscle tissue. The elastic modulus of the tumors is 5–15 times that of normal tissue. In order to compare with the simulation results of the above structure, we also designed another structure to perform the same simulation as shown in Fig. 5(a), which directly adheres the PZT patch on the injection needle.

The changes of contact angle can be divided into two types, one is 'front', which will increase the contact angle between the injection needle and the tissue sample (+); the other is 'back', which will decrease the contact angle between the injection needle and the tissue sample (−). We set up seven contact models with contact angles of −15°, −10°, −5°, 0°, 5°, 10°, and 15°, shown in Fig. 6(a–c). The simulation results are shown in Fig. 7 and Fig. 8.

Table 3. Sample number and hardness

Sample number	Hardness (MPa)
1	0.045
2	0.157
3	0.228
4	0.414
5	0.6

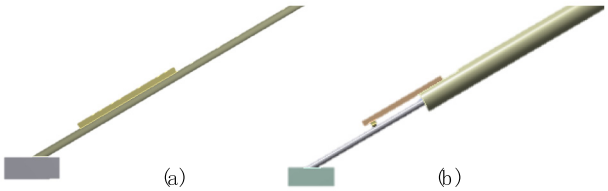

Fig. 5. (a) Structure A. (b) Structure B.

From Fig. 7, we can see that compared with structure B, structure A is more easily affected by the change of contact angle. Then, in order to better show the performance difference between the two structures, we can calculate the frequency change ratio (R) according to the following equation:

$$R = \frac{f_r^{\alpha} - f_r^{0}}{f_r^{\alpha}} \tag{2}$$

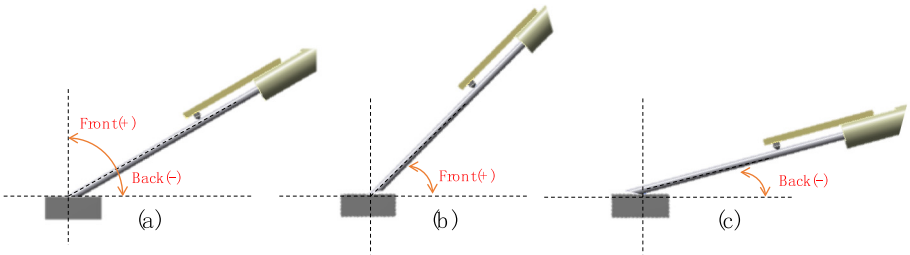

Fig. 6. (a) Ideal contact model. (b) 'front' contact model. (c) 'back' contact model

Where f_r^{α} refers to the resonant frequency of the sensor under different contact angles and f_r^0 refers to the resonant frequency of the sensor at 0° contact angle. The results are shown in Fig. 8.

It can be seen that the structure A is greatly affected by the contact angle, and the frequency change rate is 15% to 30%. It is not conducive for the sensor to recognize tissues of different hardness. As shown in Fig. 8(b), the frequency change rate of the structure B is 3% to 7%. It is much smaller than the structure A, which shows that the structure designed in the paper has a certain improvement effect in dealing with the impact of different contact angles on the performance of the sensor. At the same time, we found that under the same angle of change of the two changing methods, the change of resonant frequency is similar, and the error can be ignored.

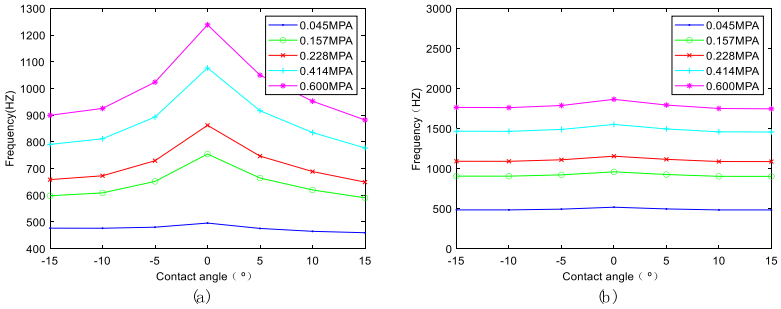

Fig. 7. (a) Contact angle-frequency curve of structure A. (b) Contact angle-frequency curve of structure B.

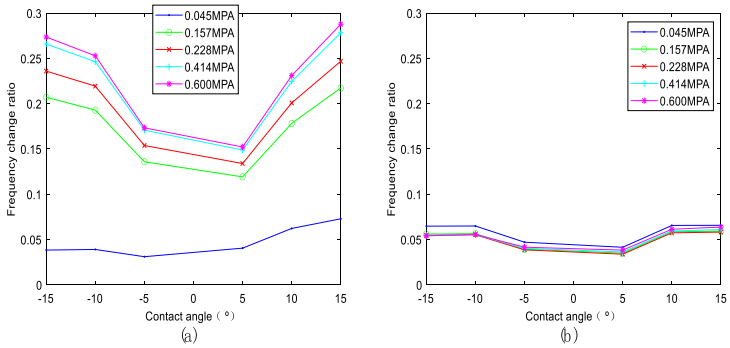

Fig. 8. (a) Frequency change ratio of structure A. (b) Frequency change ratio of structure B.

4 Intraoperative Autonomous Tumor Boundary Recognition

A tumor boundary recognition algorithm is proposed to use the above developed tactile sensor for robotic autonomous tumor localization and boundary identification.

4.1 The Boundary Recognition Function

The boundary recognition function is used to select the point to detect. After enough points have been detected, the final hardness distribution map can be obtained and the boundary is clear enough to guide tumor resection. The boundary recognition function is based on two strategies: exploration and exploitation. The functions of these two strategies are:

$$\mathbf{x}_t = \arg\max_{\mathbf{x}\in T}(\sigma_{t-1}(\mathbf{x})) \tag{3}$$

$$\mathbf{x}_t = \arg\max_{\mathbf{x}\in T}(\mu_{t-1}(\mathbf{x})) \tag{4}$$

$\mu(x)$ is the average of the predicted output. $\sigma^2(x)$ is the variance of the predicted output. The exploration function aims at exploring unknown areas and the exploitation function aims at exploiting areas of interest. Combining (3) and (4), the tumor boundary recognition function is:

$$\mathbf{x}_t = \arg\max_{\mathbf{x}\in T}((1-\theta) * \sigma_{t-1}(\mathbf{x}) - \theta * |\mu_{t-1}(\mathbf{x}) - h_{t-1}|) \tag{5}$$

where θ is a weight coefficient, h_{t-1} represents the hardness on the tumor boundary.

4.2 Simulation Process

A virtual sample with surface discretization is divided into three regions according to its hardness: tumor interior, tumor boundary and normal tissue. The shape of tumor is set as a circle. The number of sampling point is N = 100. The input is point coordinate and hardness; the algorithm uses the known information to calculate the next optimal point to detect; the output is the hardness distribution map of target area. The F_1 score [10] is used to evaluate the quality of recognition:

$$F_1 = 2 \times \frac{\text{Precision} \times \text{Recall}}{\text{Precision} + \text{Recall}} \in [0, 1] \tag{6}$$

By adjusting θ, obtaining the maximum F_1 value, and the θ at this time is substituted into the algorithm.

Flow diagram of the tumor boundary recognition algorithm is shown in Fig. 9.

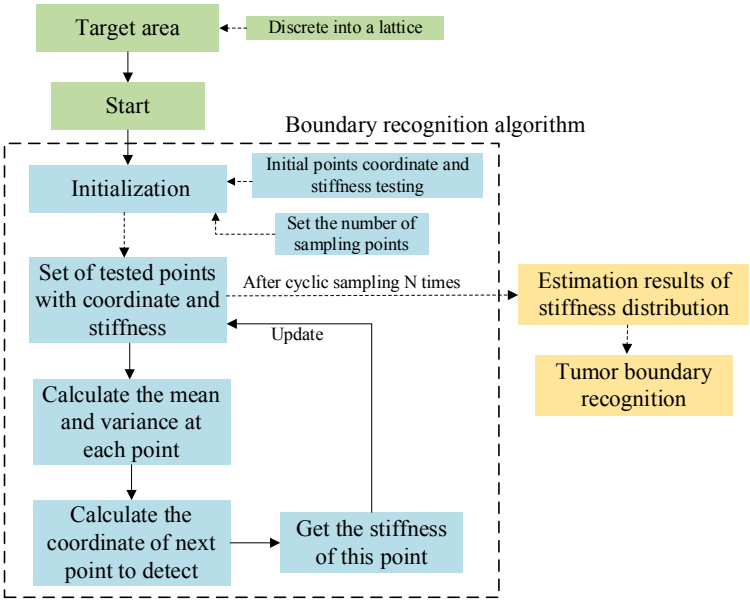

Fig. 9. Flow diagram of the tumor boundary recognition algorithm.

4.3 Results and Discussion

Set θ around 0.5 (= 0.4, 0.5, 0.6, 0.7) to balance exploration and exploitation. The corresponding F_1 score is shown in Fig. 10.

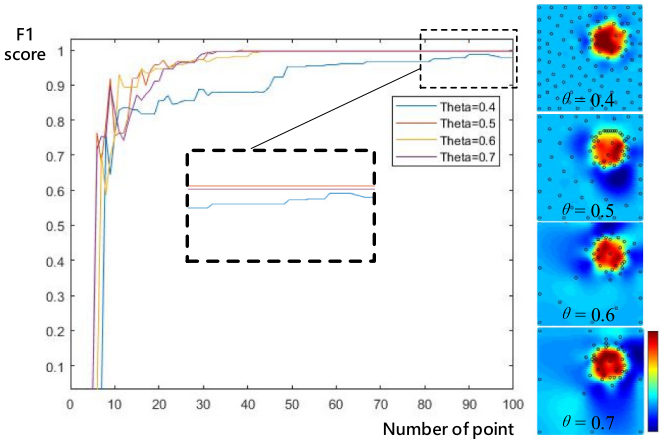

Fig. 10. F1 score corresponding to different θ.

Obviously, the F_1 score obtained 1 (maximum value) when $\theta = 0.5$. So $\theta = 0.5$ is used in the next simulation.

Two shapes of tumor sample are used to test the tumor boundary recognition algorithm. The hardness distribution maps of three different functions are shown in Fig. 11.

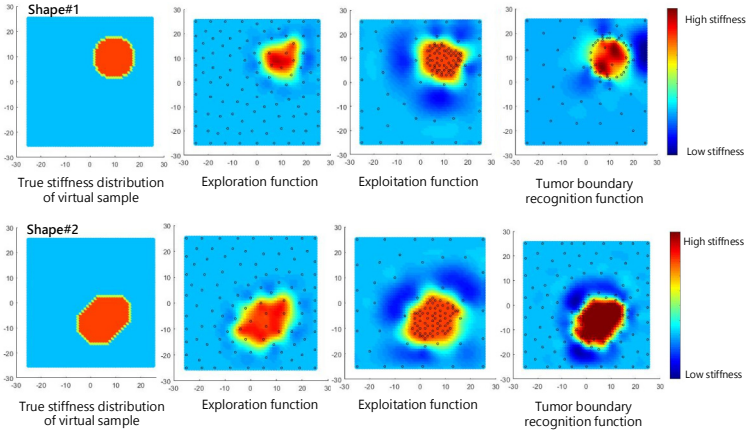

Fig. 11. Tumor recognition result.

It can be seen from Fig. 11 that the boundary of tumor can be clearly recognized using the tumor boundary recognition function. The exploration function can't maintain sampling points around the tumor. The exploitation function can find tumor and sample around it easily but can't recognize the boundary clearly.

5 Conclusions

This paper presents a tactile sensor integrated onto an endoscopic injection needle and a tumor boundary palpation algorithm. The tactile sensor is based on piezoelectric effect, which can effectively detect the hardness of tissue. Moreover, the performance of the sensor is less affected by the contact angle between the needle sheath and the tissue. In addition, a tumor boundary recognition algorithm is applied to estimate tissue hardness distribution. Compared with existing tumor detection algorithms, the simulation results show that the boundary recognition algorithm can accurately detect the location and shape of tumor in tissue samples, which is better than the exploration strategy and the exploitation strategy.

Acknowledgements. This work is supported by National Natural Science Foundation of China (No. 61973335 and No. 62111530151), Natural Science Foundation of Jiangsu Province (BK20191272) and Postgraduate Research & Practice Innovation Program of Jiangsu Province (SJCX21_0096).

References

1. Morizane, S., Honda, M., Ueki, M., Masumori, N., Fujimiya, M., Takenaka, A.: New technique of transurethral en bloc resection of bladder tumor with a flexible cystoscope and endoscopic submucosal dissection devices for the gastrointestinal tract. Int. J. Urol. **27**, 268–269 (2020). https://doi.org/10.1111/iju.14169
2. Zareinia, K., et al.: A force-sensing bipolar forceps to quantify tool-tissue interaction forces in microsurgery. IEEE/ASME Trans. Mechatron. **21**(5), 2365–2377 (2016)
3. Sharma, S., Aguilera, R., Rao, J., Gimzewski, J.K.: Piezoelectric needle sensor reveals mechanical heterogeneity in human thyroid tissue lesions. Sci. Rep. **9**(1), 9282 (2019)
4. Kim, U., Kim, Y.B., So, J., Seok, D.-Y., Choi, H.R.: Sensorized surgical forceps for robotic–assisted minimally invasive surgery. IEEE Trans. Ind. Electron. **65**(12), 9604–9613 (2018)
5. Tanaka, Y., Fukuda, T., Fujiwara, M., et al.: Tactile sensor using acoustic reflection for lump detection in laparoscopic surgery. Int. J. Comput. Assist. Radiol. Surg. **10**(2), 183–193 (2014)
6. Li, T., Pan, A., Ren, H.: Reaction force mapping by 3-axis tactile sensing with arbitrary angles for tissue hard-inclusion localization. IEEE Trans. Biomed. Eng. **68**, 26–35 (2020)
7. Ju, F.: A piezoelectric tactile sensor and human-inspired tactile exploration strategy for lump palpation in tele-operative robotic minimally invasive surgery. In: Proceedings of the 2019 IEEE International Conference on Robotics and Biomimetics (ROBIO), Dali, China, 6–8 December 2019, pp. 223–228 (2019)
8. Uribe, D.O., Schoukens, J., Stroop, R.: Improved tactile resonance sensor for robotic assisted surgery. Mech. Syst. Signal Process. **99**, 600–610 (2018)

9. Ju, F., Wang, Y., Zhang, Z., et al.: A miniature piezoelectric spiral tactile sensor for tissue hardness palpation with catheter robot in minimally invasive surgery. Smart Mater. Struct. **28**, 025033 (2019)
10. Yun, Y., Ju, F., Zhang, Y., et al.: Palpation-based multi-tumor detection method considering moving distance for robot-assisted minimally invasive surgery. In: 2020 42nd Annual International Conference of the IEEE Engineering in Medicine & Biology Society (EMBC), Montreal, QC, Canada, pp. 4899–4902 (2020). https://doi.org/10.1109/EMBC44109.2020.9176127